Nanoscale

PAPER

View Article Online
View Journal

Thermoelectric voltage measurements of atomic and molecular wires using microheater-embedded mechanically-controllable break junctions

Cite this: DOI: 10.1039/c4nr00127c

Takanori Morikawa, Akihide Arima, Makusu Tsutsui* and Masateru Taniguchi*

Received 8th January 2014
Accepted 14th May 2014

DOI: 10.1039/c4nr00127c

www.rsc.org/nanoscale

We developed a method for simultaneous measurements of conductance and thermopower of atomic and molecular junctions by using a microheater-embedded mechanically-controllable break junction. We find linear increase in the thermoelectric voltage of Au atomic junctions with the voltage added to the heater. We also detect thermopower oscillations at several conductance quanta reflecting the quantum confinement effects in the atomic wire. Under high heater voltage conditions, on the other hand, we observed a peculiar behaviour in the conductance dependent thermopower, which was ascribed to a disordered contact structure under elevated temperatures.

Introduction

Thermoelectric devices are considered as one of the ideal systems for energy harvesting that can directly convert heat energy into electricity. The crucial issue in practical applications of thermoelectric power generation has been the low energy conversion efficiency, which is characterized by the dimensionless figure of merit $ZT = \sigma S^2/\kappa$ of the material used, where σ, S, and κ are the electrical conductivity, the Seebeck coefficient, and the thermal conductivity.[1–3] Because the three properties are mutually correlated with each other, it is difficult to achieve high ZT in bulk crystals.[1–3]

Recently, there has been increasing interest in exploiting quantum effects as a new venue for developing high ZT materials.[4–12] One of the promising outcomes of this novel approach is the sharp increase in the electronic density of states near the Fermi level in the low-dimensional materials that can provide enhanced thermopower.[5–7] This concept has been confirmed experimentally in nanostructures, such as PbSeTe/PbTe quantum dot superlattices[8] and InAs nanowires.[9,10] In this context, atomic and molecular wires, a quantum system consisting of single or a few atoms or molecules connected to two electrodes, can also be a good candidate for the new class of thermoelectric materials that leverages quantum confinement effects.[13–18] To date, thermopower measurements of Au atomic junctions have been achieved at a cryogenic temperature.[19] Recently, it has also become technically feasible to assess the thermoelectric power of a few[16] or individual molecules.[17,20] There are, however, no reliable tools for evaluating the size effects of the thermoelectric transport in atomic contacts due to the technical difficulty to create a stable nanojunction and control the atomic structure with sub-nanoscale resolution under ambient conditions.

In the present study, therefore, we developed a method to measure thermoelectric properties of a size-variable atomic junction at room temperatures. Our approach is based on a self-breaking technique[21,22] using a micro-fabricated mechanically-controllable break junction (MCBJ)[23] that is capable of forming stable junctions and manipulating the mechanical deformation to change their size at the atomic level.[21,22] In order to make use of this technique for thermopower measurements of atomic wires, and molecular junctions if possible, a microheater was embedded in the MCBJs[24] for imposing a temperature gradient to generate measurable thermoelectric voltage at the junction.

Experimental

Fabrication of heater-embedded MCBJs

Heater-embedded MCBJs were fabricated as follows.[24] First, a 0.5 mm thick phosphor bronze substrate was coated with a 4 μm polyimide layer by spin coating imide monomer solution followed by baking at 200 degrees Celsius on a hot plate. We then patterned microelectrodes by photolithography with an AZ-5206E resist. After development, Au of thickness 30 nm with a 1 nm Cr adhesion layer was deposited by radio-frequency magnetron sputtering. The residual resist was removed by immersing the sample in *N*,*N*-dimethylformamide overnight and sonication. Using a part of the thus created electrodes as external markers, we delineated squares by an electron beam drawing using a ZEP520A-7 resist. Subsequently, a 20 nm thick Al_2O_3 layer was deposited. After the lift-off, we obtained Al_2O_3 islands onto which microheaters and nanojunctions were formed through the same nanofabrication processes. Here, the microheaters consisted of Pt coils with a 300 nm line-space

The Institute of Scientific and Industrial Research, Osaka University, 8-1 Mihogaoka, Ibaraki, Osaka 567-0047, Japan. E-mail: tsutsui@sanken.osaka-u.ac.jp; taniguti@sanken.osaka-u.ac.jp; Fax: +81-6-6875-2440; Tel: +81-6-6879-8447

geometry, whose local temperature can be controlled *via* Joule heating through adjusting the voltage V_h.[24] On the other hand, the junction was made of 100 nm thick Au on a 1 nm thick Cr layer and designed to have a bow-tie shape of cross-section area 100 nm × 100 nm at the narrowest constriction. After fabricating all the components, the substrate was exposed to reactive ion etching at 50 W with O_2 etchant gas. As a result, the polyimide underneath the junction was removed.

Break junction experiments

In experiments, a heater-embedded MCBJ device was mounted on a stage in a three-point bending configuration. The sample chamber was then evacuated. When the vacuum reached below 10^{-5} Torr, the free-standing Au junction was broken at room temperatures by deflecting the substrate with a pushing rod that moves vertically by a screw mechanism (Fig. 1(a)). Meanwhile, the junction conductance G was monitored under an applied dc voltage V_b of 0.1 V using a Keithley 6487 picoammeter/source with a resistance R_s connected in series for protecting the overcurrent breakdown of the junction as depicted schematically in Fig. 1(b). After this initial breakage, the junction was recreated by reversing the screw. Thereafter, we used a piezo-actuator for fine-control of the junction elongation. In the beginning of the breaking process, G decreased gradually as the 100 nm-sized junction was thinned *via* necking deformations. When it became a few atom size, on the other hand, G started to diminish in a stepwise fashion reflecting the discrete nature of the contact mechanics that involves strain energy accumulation and contact atom rearrangements. Eventually, single-atom chains were formed, which was confirmed by observations of long plateaus at around 1 G_0.[25,26] Further bending the substrate led to fracture of the junction and drop of G to zero. After the breakdown, the junction was fused to above 15 G_0 by moving the rod in an opposite direction to release the bending force. Throughout the break junction experiments, the contact stretching speed was feedback controlled to form stable atomic contacts.[21,21]

Thermoelectric voltage and conductance measurements

During junction stretching, the thermoelectric voltage ΔV was measured in addition to G using a Keithley 2182A nanovoltometer. This was accomplished by repeating the following procedure: first recording G under $V_b = 0.1$ V and subsequently switching it to 0 V to obtain ΔV. To induce measureable thermoelectric voltage, the microheater was heated up electrically by applying a voltage V_h. All the measurements were implemented under the junction stretching speed of 0.6 pm s^{-1} below 6 G_0. The very slow elongation rate was necessary to ensure enough time for measuring ΔV with accuracy (the overall sampling rate was 3 Hz).

Results and discussions

Simultaneous measurements of conductance and thermoelectric voltage of Au atomic wires

Fig. 2(a) shows G–t and ΔV–t curves simultaneously obtained during the Au junction stretching under a constant V_h applied to the heater with the series resistance $R_s = 10$ kΩ. The thermoelectric voltage was negligibly small under low heater voltage conditions but became larger with increasing V_h as ΔV scales in proportion to the temperature gradient ΔT at the junction as $\Delta V = S\Delta T$. Moreover, it was found that ΔV was also dependent on R_s; ΔV corrected with $R_s = 10$ kΩ was smaller compared to that acquired with 100 kΩ (Fig. 2(b)), which manifests the fact that the measured ΔV is the potential drop at the series resistor. The actual thermoelectric voltage occurred at the junction ΔV_{Au} should be, therefore, deduced from the measured ΔV through $\Delta V_{Au} = \Delta V(1 + R_c/R_s)$, where $R_c = 1/G$ is the resistance of Au contacts. This indicates that the coefficient R_c/R_s determines the accuracy of the thermoelectric voltage measurement. Specifically, the measured thermoelectric voltage is close to ΔV_{Au} as long as the contact resistance is much lower than the series resistance while conversely ΔV tends to be small as R_c becomes larger than R_s. For the present case, the resistance of an Au

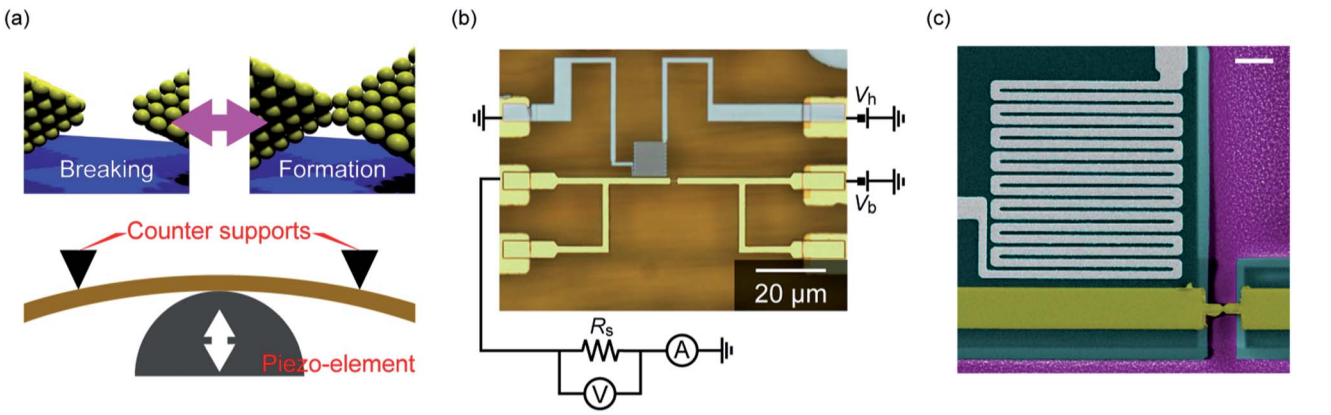

Fig. 1 Microheater-embedded MCBJ. (a) Schematic illustration of the MCBJ set up. Au atomic junctions can be formed reproducibly by the mechanical control of substrate bending through the piezo-driven pushing rod control. (b) Optical microscopic image of a microheater-embedded MCBJ consisting of a Pt coil (grey) and a free-standing Au junction (yellow) on a polyimide-coated phosphor bronze substrate. (c) False-colored scanning electron micrograph of the microheater and the Au junction. The cyan colored region is the Al_2O_3 layer that served as a heat bath for imposing a temperature gradient on the junction *via* Joule heating of the Pt microheater. Scale bar denotes 2 μm.

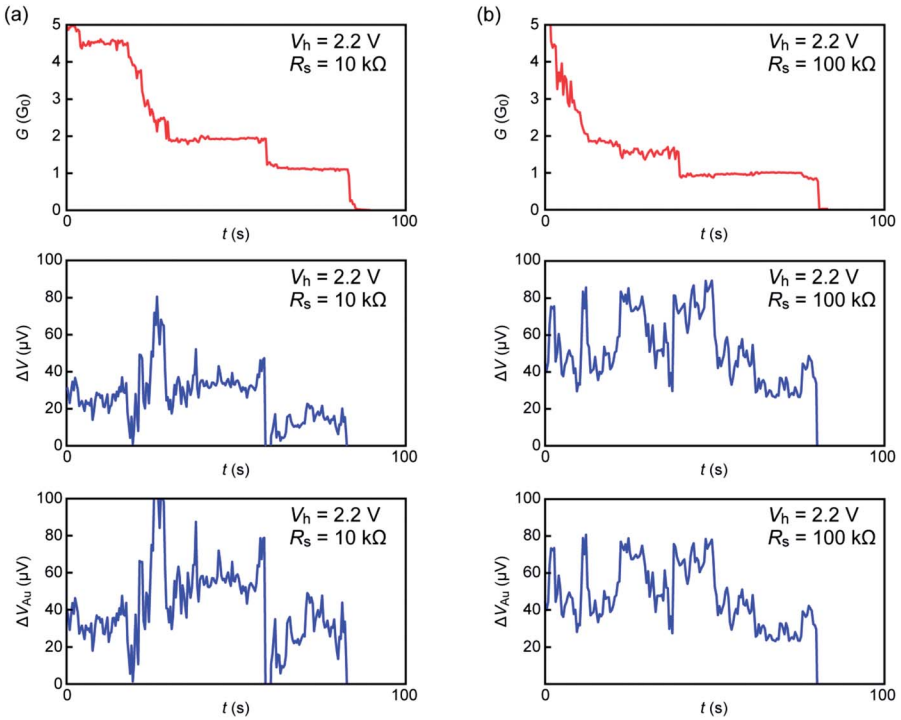

Fig. 2 The traces of conductance G (top), the as-obtained thermoelectric voltage ΔV (middle), and the actual thermoelectric voltage at the Au junction ΔV_{Au} measured with a sensing resistance of (a) $R_s = 10$ kΩ and (b) $R_s = 100$ kΩ.

junction changes in a range from 100 Ω to around 10 kΩ during the course of breaking processes. Thus, ΔV becomes less than 1/10 of ΔV_{Au} when 1 kΩ series resistance was used, which makes it difficult to evaluate the quantum effects on the thermopower. In contrast, a 10 kΩ sensing resistor gives ΔV that is close to ΔV_{Au} at $R_c <$ several kΩ but still gets small to about $\Delta V_{Au}/2$ when R_c is above 10 kΩ. In this sense, it is better to use 100 kΩ series resistance for the thermoelectric voltage measurements. However, it should be noted that a high resistance connected in series also has a drawback in that it makes estimations of the junction conductance difficult when $R_c \ll R_s$. As the junction conductance at $G > 1\ G_0$ is an important parameter for controlling the contact mechanics, it means R_s cannot be made so large (we found that it needs to be smaller than 200 kΩ in our system). Therefore, there is a trade-off in choosing what external resistance to use.

Quantum size effects in thermopower of Au quantum wires

We now focus on the size effects of the thermopower of Au atomic junctions. This can be examined by evaluating the conductance dependence of the thermoelectric voltage as G is essentially in proportion to the size of the contact.[26] Scatter plots of ΔV_{Au} *versus* G acquired with a 100 kΩ sensing resistor shows scattering of data at a low conductance regime below several conductance quanta (Fig. 3(a)).[19,27] Interestingly, a conductance dependent oscillation of the thermoelectric voltage showing local minima at multiple integers of 1 G_0 becomes observable at the conductance lower than 4 G_0 when taking the average of ΔV_{Au} in a conductance window of 0.05 G_0

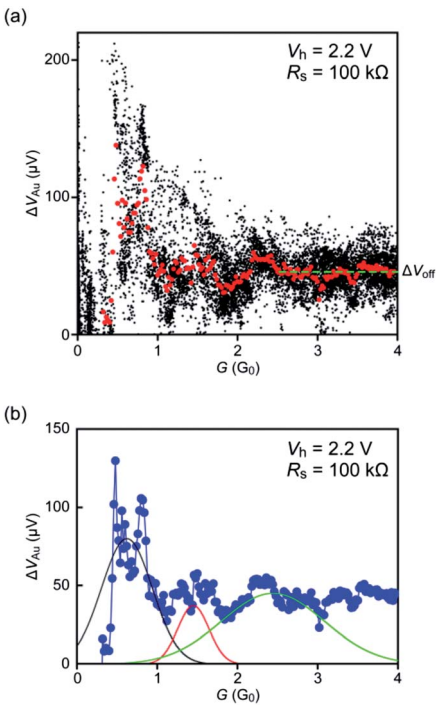

Fig. 3 Thermopower oscillation in an Au atomic wire. (a) ΔV_{Au} *versus* G scatter plots showing data obtained with a 100 kΩ sensing resistor R_s. The red plots are the average values. (b) Average ΔV_{Au} plotted against G. The solid curves are Gaussian fits to the plots.

and plotting it against G (Fig. 3(b)). This distinct behaviour reflects the one-dimensional band structure in the virtually ideal electron waveguide of the ballistic Au atomic wires.[28–31] It is also noticeable that the sign of the thermopower $S = -\Delta V_{Au}/\Delta T$ is negative for the Au atom-sized contacts in contrast to the positive Seebeck coefficient of its bulk counterpart, which also agrees with the quantized thermopower predicted by Landauer theory.[28] These characteristic features represent that the quantum nature in the ballistic Au wires becomes observable when the size is narrowed to be comparable to the Fermi wavelength during the junction stretching, alike conductance quantization in metallic nanocontacts.

Then, it is interesting to note that while the thermopower of a fully-transparent quantum wire should be close to zero,[28] the measured thermovoltage shows relatively high values even at conductance quanta (Fig. 2 and 3). The non-zero ΔV_{Au} is presumably the thermoelectric voltage arising at bulk regions of Au junctions as explained in the following. When the microheater was electrically heated by the applied voltage of $V_h = 2.2$ V, the local temperature in the vicinity of Au single-atom contacts T_c, estimated from the average contact lifetime[31,32] (6.2 seconds obtained from the 1 G_0 plateau length in the 50 conductance traces measured using a conductance window of 0.8 G_0 to 1.2 G_0), increased to about 312 K from the ambient $T_0 = 293$ K (Fig. 4). As a result, a temperature difference is established over an Au atomic junction up to 19 K as the thermal conductance of an atomic chain (10^{-11} W K^{-1})[33,34] is significantly lower than that of bulk regions ($\sim 10^{-5}$ W K^{-1}, roughly estimated from bulk thermal conductivity of Au (320 W mK^{-1}), wire width (400 nm), thickness (100 nm) and length (1 μm)). On the other hand, resistance measurements of the microheater suggested that the temperature at the Pt coil T_h is raised to around 402 K.[31] This indicates a substantial temperature difference established in the micrometer-long Au wire as well (Fig. 4). Thermoelectric voltage occurring at the contact bank is, therefore, included in the measured ΔV_{Au}. In fact, the bulk contribution was detected as an offset, ΔV_{off} (Fig. 3(a)). Moreover, we confirmed that average ΔV_{off} tends to change a little with the conductance at $G > 4$ G_0 but increases quadratically with V_h. This is reasonable as the microstructure of the bulk region is little affected during stretching of Au junctions (tensile force tends to be concentrated at the narrowed constriction and hence does not induce mechanical deformation of the micrometer-long Au wire). Thermoelectric voltage was eventually lifted by ΔV_{off} on average, thereby leading to the virtually nonzero thermovoltage at quantized conductance.

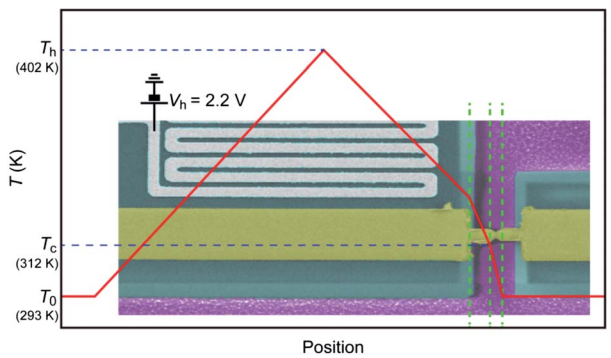

Fig. 4 Conceptual temperature profile. T_h, T_c, and T_0 denote the local temperature at the microheater, the temperature at the atomic contact, and the ambient temperature, respectively. The red curve illustrates temperature differences established in the Au junction.

As ΔV_{Au} includes the bulk contribution in addition to the thermoelectric voltage created at the atomic wire, it is worth discussing what is actually observed in detail (for instance in the traces shown in Fig. 2). For this, we would like to note that in many cases the thermovoltage and the conductance show steps at the same point. Meanwhile, the junction conductance in the several-G_0 range is determined predominantly by the atomic structure of Au contacts and not by the microstructure of microwire regions. Therefore, the thermovoltage steps are attributable to a change in either the electronic structure at the atom-sized contacts[19,27] during the mechanically-induced atom rearrangements in the atomic wire or ΔV_{off} due to modification in the temperature profile along the Au junction including the micro-scale regions associated with a sudden increase/decrease of the thermal conductance at the narrowest constriction. Although we cannot be definite about the cause of the step behavior at this point, our method enables to reveal the conductance-dependent thermopower oscillation by evaluating and averaging out the fluctuations in the thermoelectric properties originating from a variance in the contact geometries.

High-temperature anomaly in thermoelectric voltage of Au atomic wires

In contrast, we observed peculiar $G - \Delta V_{Au}$ characteristics when the microheater was heated to elevated temperatures. The thermoelectric voltage tended to become more negative in the wider range of the conductance by increasing the heater voltage above a certain value (Fig. 5(a)). When we observed the conductance histograms in this high-V_h regime, we found that the indication of conductance quantization, which normally gives peaks at multiple integers of 1 G_0 for the case of Au atom-sized contacts, became obscure and started to show instead a relatively broad distribution at around several conductance quanta (Fig. 5(b)). We have checked that this is unlikely to be due to any damage to the device caused by overheating of the microheater by further conducting the measurements under low-V_h conditions using the same sample to see whether the results reproduce the anomalous behaviour, wherein we obtained the characteristic peaks in the conductance histograms and the G-dependent thermopower oscillations.

The high-temperature anomaly is therefore likely to be due to the intrinsic properties of Au junctions. It is noticeable that a similar change in the peak structures of conductance histograms has been reported in the previous break junction experiments on metallic nanocontacts.[35,36] Fujii *et al.*[36] observed that the Au contacts become fragile and tend to break at high-conductance states before evolving into single- or a few-atom chains when the applied voltage exceeds a certain level, which

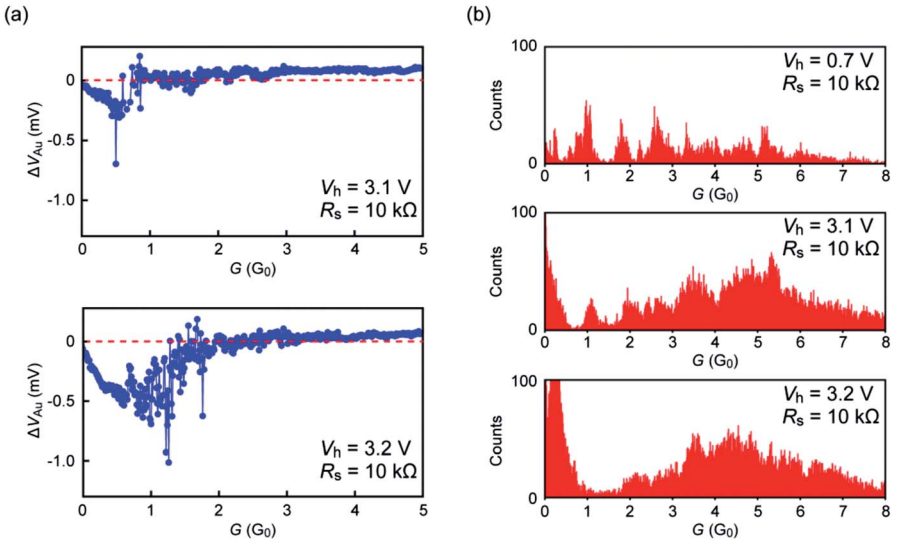

Fig. 5 Anomalous thermoelectric voltage at elevated temperatures. (a) Average plotted as a function of G for heater voltage $V_h = 3.1$ V (top) and 3.2 V (bottom). (b) Conductance histograms obtained with $V_h = 0.7$ V (top), 3.1 V (middle) and 3.2 V (bottom).

was explained to be associated with effects of local heating or electromigration.[36] To verify whether overheating can be a possible mechanism responsible for the high-temperature anomaly found in the present study, we performed high-temperature measurements of Au conductance histograms under a stretching rate condition of 0.6 nm s^{-1} in vacuum. We found in fact disappearance of the 1 G_0 features and concomitant increase in the counts at $G > 2$ G_0 in the conductance-histograms when a surrounding temperature was raised to 440 K (Fig. 6). As the applied voltage used to record G in the thermopower measurements was 0.1 V, electromigration was unlikely to cause significant influence on the contact properties. From the above results, it is likely that the anomalous $G - \Delta V_{Au}$ dependence is given as a result of local melting in atomic junctions under elevated temperatures under high-V_h conditions.

Thermopower measurements of molecular wires

We have seen so far that our method is useful for investigating thermoelectric transport through atomic wires. Beyond that, it is of interest to see whether this technique can be applied to metal–molecule–metal junctions.[13] Fig. 7(a and b) show results of the simultaneous measurements carried out on Au–1,4-benzenedithiol (BDT)–Au junctions with $R_s = 100$ kΩ in a vacuum at room temperatures. We observed plateaus at around 10^{-2} G_0 during stretching of Au junctions with BDT molecules adsorbed on the surface, which are indicative of formations of BDT single-molecule junctions.[37,38] After that, we swept the heater

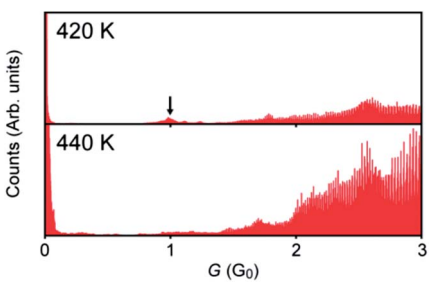

Fig. 6 Conductance histograms constructed with G–t traces recorded for Au junctions under the substrate temperature heated to 420 K (top) and 440 K (bottom). The arrow indicates the 1 G_0 peak, which disappears at 440 K.

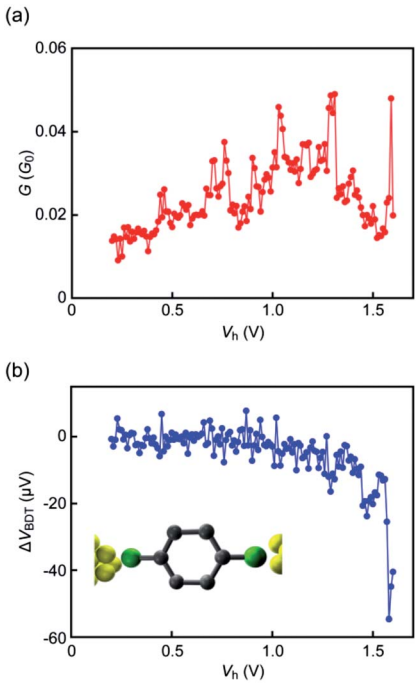

Fig. 7 Thermoelectric voltage measurements of a Au–1,4-benzenedithiol (BDT)–Au single-molecule junction. The conductance G (top) and the thermoelectric voltage ΔV_{BDT} (bottom) were recorded simultaneously while sweeping the heater voltage V_h.

voltage V_h and performed the simultaneous measurements of ΔV and G under $V_b = 0.1$ V. We observed gradual increase of ΔV_{BDT} obtained through $\Delta V_{BDT} = \Delta V(1 + R_c/R_s)$ with V_h, which is naturally ascribed to enlarged temperature gradient at the junction (Fig. 7(b)).

It is noted that the thermovoltage fluctuates significantly and even changes its sign at some points. The large variation in ΔV_{BDT} is attributed to a change in transmission curve line shapes associated with modifications of metal–molecule contact geometries.[39] This is in fact very likely to happen as the gradual increase in the heater temperature would cause thermal expansion of Au during the measurement that tends to close the junction.

Single-molecule thermopower can be estimated, in principle, from ΔV_{BDT} measured. As mentioned earlier, the local temperature T_c in the vicinity of the junction can be deduced from the V_h-dependence of the lifetime of the Au single-atom contacts $\tau = f_0^{-1} \exp(-E_b/k_B T_c)$.[21,40] Assuming $T_c \sim {V_h}^2$, which should be valid in the present case where thermal conduction through the heat-conductive Au leads is a predominant factor over others such as radiation and convection,[41] we obtained the T_c–V_h relationship. Using the thus acquired T_c and taking the cold side of the junction at the ambient $T_0 = 293$ K, thermopower of BDT S_{BDT} is calculated as $S_{BDT} = -\Delta V_{BDT}/(T_c - T_0)$, which yields an average thermopower of 1.4 μV K^{-1}. The positive thermoelectric power on average reflecting the electron tunnelling through the HOMO of the molecule is in agreement with the previous experiment.[16] The sixfold smaller value is probably due to a difference in the Au–BDT–Au junction configurations.[42] This suggests a possible use of the present system for evaluating the thermopower of metal–molecule–metal junctions.

Conclusions

A method was described for evaluating thermoelectric transport characteristics of atomic and molecular wires connected to two electrodes. We performed simultaneous measurements of the thermoelectric voltage and conductance of Au atom-sized contacts using a microheater-embedded MCBJ. We observed a negative thermopower in Au atomic chains at a low-V_h regime reflecting the quantum nature of thermoelectric effects in the one-dimensional quantum conductor as an ideal electron waveguide. In sharp contrast, positive thermopower was found under elevated heater voltage conditions presumably due to junction overheating that led to formation of disordered Au nanocontacts. The measurements were also applied to BDT single-molecule junctions, wherein we obtained positive thermopower suggestive of electron transmission through the HOMO. The present study proves the potential use of the microheater-embedded MCBJs for evaluating the thermoelectric properties of atomic and molecular wires.

Acknowledgements

This research was supported in part by the Strategic Information and Communications R&D Promotion Programme (122107001) of the Ministry of Internal Affairs and Communications and the "Nanotechnology Platform Project (Nanotechnology Open Facilities in Osaka University)" of the Ministry of Education, Culture, Sports, Science and Technology, Japan [no. F-12-OS-0016]. M. Tsutsui acknowledges support from the Yazaki Memorial Foundation for Science and Technology, Tanigawa Fund Promotion of Thermal Technology, the Inamori Foundation, and the Asahi Glass Foundation.

Notes and references

1 J. R. Sootsman, D. Y. Chung and M. G. Kanatzidis, *Angew. Chem., Int. Ed.*, 2009, **48**, 8616–8639.
2 M. Zebarjadi, K. Esfarjani, M. S. Dresselhaus, Z. F. Ren and C. Gang, *Energy Environ. Sci.*, 2012, **5**, 5147–5162.
3 M. H. Elsheikh, D. A. Shnawah, M. F. M. Sabri, S. B. M. Said, M. H. Sassan, M. B. A. Bashir and M. Mohamad, *Renewable Sustainable Energy Rev.*, 2014, **30**, 337–355.
4 L. D. Hicks and M. S. Dresselhaus, *Phys. Rev.*, 1993, **47**, 16631–16634.
5 G. D. Mahan and J. O. Sofo, *Proc. Natl. Acad. Sci. U. S. A.*, 1996, **93**, 7436–7439.
6 M. S. Dresselhaus, G. Chen, M. Y. Tang, R. Yang, H. Lee, D. Wang, Z. Ren, J.-P. Fleurial and P. Gogna, *Adv. Mater.*, 2007, **19**, 1043–1053.
7 K. Raseong, S. Datta and M. S. Lundstorm, *J. Appl. Phys.*, 2009, **105**, 034506.
8 T. C. Harman, P. J. Taylor, M. P. Walsh and B. E. LaForge, *Science*, 2002, **297**, 2229.
9 Y. Tian, M. R. Sakr, J. M. Kinder, D. Liang, M. J. MacDonald, R. L. J. Qiu, H.-J. Gao and X. P. A. Gao, *Nano Lett.*, 2012, **12**, 6492.
10 P. M. Wu, J. Gooth, X. Zianni, S. F. Svensson, J. G. Gluschke, K. A. Dick, C. Thelander, K. Nielsch and H. Linke, *Nano Lett.*, 2013, **13**, 4080.
11 C. J. Vineis, A. Shakouri, A. Majumdar and M. G. Kanatzidis, *Adv. Mater.*, 2010, **22**, 3970–3980.
12 J. P. Heremans, M. S. Dresselhaus, L. E. Bell and D. T. Morelli, *Nat. Nanotechnol.*, 2013, **8**, 471–473.
13 Y. Dubi and M. Di Ventra, *Rev. Mod. Phys.*, 2011, **83**, 131–155.
14 M. Tsutsui and M. Taniguchi, *Sensors*, 2012, **12**, 7259–7298.
15 J. A. Malen, S. K. Yee, A. Majumdar and R. A. Segalman, *Chem. Phys. Lett.*, 2010, **491**, 109–122.
16 P. Reddy, S.-Y. Jang, R. A. Segalman and A. Majumdar, *Science*, 2007, **315**, 1568–1571.
17 J. R. Widawsky, P. Darancet, J. B. Neaton and L. Venkataraman, *Nano Lett.*, 2011, **12**, 354–358.
18 E. Shapira, A. Holtzman, D. Marchak and Y. Selzer, *Nano Lett.*, 2012, **12**, 808–812.
19 B. Ludoph and J. M. van Ruitenbeek, *Phys. Rev. B: Condens. Matter Mater. Phys.*, 1999, **59**, 12290–12293.
20 S. Guo, G. Zhou and N. Tao, *Nano Lett.*, 2013, **13**, 4326–4332.
21 M. Tsutsui, K. Shoji, M. Taniguchi and T. Kawai, *Nano Lett.*, 2008, **8**, 345–349.
22 M. Tsutsui, M. Taniguchi and T. Kawai, *Nano Lett.*, 2009, **9**, 2433–2439.
23 J. M. van Ruitenbeek, A. Alvarez, I. Pineyro, C. Grahmann, P. Joyez, M. H. Devoret, D. Esteve and C. Urbina, *Rev. Sci. Instrum.*, 1996, **67**, 108–111.

24 M. Tsutsui, T. Kawai and M. Taniguchi, *Sci. Rep.*, 2012, **2**, 217.
25 H. Ohnishi, Y. Kondo and K. Takayanagi, *Nature*, 1998, **395**, 780–783.
26 N. Agraït, A. L. Yeyati and J. M. van Ruitenbeek, *Phys. Rep.*, 2003, **377**, 81–279.
27 F. Pauly, J. K. Viljas, M. Burkle, M. Dreher, P. Nielaba and J. C. Cuevas, *Phys. Rev. B: Condens. Matter Mater. Phys.*, 2011, **84**, 195420.
28 H. van Houten, L. W. Molenkamp, C. W. J. Beenakker and C. T. Foxon, *Semicond. Sci. Technol.*, 1992, **7**, B215–B221.
29 B. J. van Wees, H. van houten, C. W. Beenakker, J. G. Williamson, L. P. Kouwenhoven, D. van der Marel and C. T. Foxon, *Phys. Rev. Lett.*, 1998, **60**, 848–850.
30 A. S. Dzurak, C. G. Smith, L. Martin-Moreno, M. Pepper, D. A. Ritchie, G. A. C. Jones and D. G. Hasko, *J. Phys.: Condens. Matter*, 1993, **5**, 8055–8064.
31 M. Tsutsui, T. Morikawa, A. Arima and M. Taniguchi, *Sci. Rep.*, 2013, **3**, 3326.
32 M. Tsutsui, M. Taniguchi and T. Kawai, *Nano Lett.*, 2008, **8**, 3293–3297.
33 A. Ozpineci and S. Ciraci, *Phys. Rev. B: Condens. Matter Mater. Phys.*, 2001, **63**, 125415.
34 L. W. Molenkamp, Th. Gravier, H. van Houten, O. J. A. Buijk, M. A. Mabesoone and C. T. Foxon, *Phys. Rev. Lett.*, 1992, **68**, 3765.
35 H. Yasuda and A. Sakai, *Phys. Rev. B: Condens. Matter Mater. Phys.*, 1997, **56**, 1069–1072.
36 A. Fujii, M. Tsutsui, S. Kurokawa and A. Sakai, *Phys. Rev. B: Condens. Matter Mater. Phys.*, 2005, **72**, 045407.
37 X. Bingqian and N. J. Tao, *Nano Lett.*, 2004, **4**, 267–271.
38 M. Tsutsui, M. Taniguchi and T. Kawai, *Nano Lett.*, 2008, **8**, 3293–3297.
39 Y. Dubi and M. Di Ventra, *Nano Lett.*, 2009, **9**, 97.
40 M. Tsutsui, T. Ohshiro, K. Matsubara, M. Furuhashi, M. Taniguchi and T. Kawai, *J. Appl. Phys.*, 2010, **108**, 064312.
41 H. Zheng, A. Cao, C. R. Weinberger, J. Y. Huang, K. Du, J. Wang, Y. Ma, Y. Xia and S. X. Mao, *Nat. Commun.*, 2010, **1**, 144.
42 S. Y. Quek, H. J. Choi, S. G. Louie and J. B. Neaton, *ACS Nano*, 2011, **5**, 551–557.